EUROPEAN ORGANIZATION FOR NUCLEAR RESEARCH

CERN/EP 85-33
18 March 1985

A STUDY OF SINGLE MESON PRODUCTION IN NEUTRINO AND ANTINEUTRINO CHARGED CURRENT INTERACTIONS ON PROTONS

Aachen-Birmingham-Bonn-CERN-London I.C.-Munich (MPI)-Oxford Collaboration

P. Allen(*), H. Grässler and R. Schulte
III. Physikalisches Institut der Technischen Hochschule, Aachen, Germany

G.T. Jones, B.W. Kennedy, S.W. O'Neale
University of Birmingham, UK

W. Gebel and E. Hofmann
Physikalisches Institut der Universität Bonn, Bonn, Germany

H. Klein, J. Mittendorfer(**), D.R.O. Morrison, P. Schmid, H. Wachsmuth
CERN, European Organization for Nuclear Research, Geneva, Switzerland

K.W.J. Barnham, E.F. Clayton, F. Hamisi, D.M. Miller and M.M. Mobayyen
Imperial College of Science and Technology, London, UK

M. Aderholz, L. Deck, N. Schmitz and W. Wittek
Max-Planck-Institut für Physik und Astrophysik, München, Germany

G. Corrigan, G. Myatt, D. Radojicic, B. Saitta(***), P.N. Shotton and S.J. Towers
Department of Nuclear Physics, Oxford, UK

Submitted to Nuclear Physics B

(*) Now at Physics Dept., Brown University, Providence, Rhode Island, USA.

(**) Now at Höhere Technische Lehranstalt, Wels, Austria.

(***) Now at Istituto Nazionale di Fisica Nucleare, Pisa, Italy.

EP/2127P/PS/ed

ABSTRACT

We present results on exclusive single charged pion and kaon production in neutrino and antineutrino interactions on protons in the energy range from 5 to 120 GeV. The data were obtained from exposures of BEBC to wide band beams at the CERN SPS. For invariant masses of the ($p\pi$) system below 2 GeV, the pions originate predominantly from decays of baryon resonances excited by the weak charged current. Similarly, we observe the production of $\Lambda(1520)$ decaying into p and K^-. For invariant masses above 2 GeV pion production becomes peripheral by interaction of the weak current with a virtual π^o. We establish a contribution of longitudinally polarised intermediate vector bosons to this process.

1. INTRODUCTION

One-pion production in neutrino and antineutrino charged current interactions has been studied in the past both theoretically and experimentally. Since exclusive channels are best studied in bubble chambers and because of the small production cross sections, data samples are small. Comparison with models gave general agreement but could not test detailed assumptions.

Most of the previous work has concentrated on $\Delta^{++}(1232)$ production in the reaction

$$\nu p \rightarrow \mu^- p \pi^+ . \qquad (1)$$

Data exist both from low energy ($\langle E_\nu \rangle \sim 2$ GeV) [1-4] and high energy experiments ($\langle E_\nu \rangle \sim 20$ GeV) [5,6,9].

Three experiments have published data on the corresponding antineutrino reaction

$$\bar{\nu} p \rightarrow \mu^+ p \pi^- . \qquad (2)$$

At low antineutrino energies, 246 events were found in the Gargamelle heavy liquid bubble chamber [7]. Barish et al. [8] have analysed 175 events of this reaction at high energies obtained in the 15' bubble chamber at FNAL. Recently Allasia et al. [9] have published results from antineutrino interactions with deuterium in BEBC. They were able to study reaction (2) in the presence of a spectator neutron.

This work describes data obtained since 1977 in the wide band neutrino and antineutrino experiments at the CERN SPS using BEBC filled with hydrogen. The data sample analysed until now consists of 1155 events of reaction (1) and 375 events of reaction (2). The energy of both the neutrino and antineutrino beams generating these events ranges from 5 to 120 GeV, the mean event energy being about 25 GeV.

Reactions (1) and (2) are similar in that baryonic resonances dominate the distribution of the effective mass, W, of the hadronic ($p\pi$) system from threshold up to about 2 GeV, whereas at larger masses the pions appear to be produced by a peripheral mechanism. Because of the different isospin

content of the final states, the resonances produced in ν and $\bar{\nu}$ interactions are very different. On the other hand, we will show that for W > 2 GeV the reaction is essentially the same for ν and $\bar{\nu}$. Because of this we discuss the neutrino and antineutrino induced reactions together but divide them into a low mass (W < 2 GeV) and a high mass (W > 2 GeV) region.

We have already published [6] a detailed study of $\Delta^{++}(1232)$ production in reaction (1) using about 60% of the present data sample. In sect. 3.1 we will, therefore, concentrate on the new antineutrino data showing corresponding data of reaction (1) for comparison. In sect. 3.2 the high mass samples resulting from reactions (1) and (2) will be compared and eventually combined for studies of the reaction mechanism.

As the weak charged current is not flavour-conserving, one also expects single kaon production to occur in neutrino and antineutrino interactions:

$$\nu p \rightarrow \mu^- p K^+ \qquad (3)$$

$$\bar{\nu} p \rightarrow \mu^+ p K^- \quad . \qquad (4)$$

These reactions are Cabbibo-suppressed and therefore less frequent than reactions (1) and (2) by at least one order of magnitude. Unique fits to these reactions will be discussed in sect. 3.3.

2. THE EXPERIMENT

The complete experiment consists of several exposures of the Big European Bubble Chamber (BEBC) to wide band ν or $\bar{\nu}$ beams. The experiment started in 1977 with a neutrino exposure at a proton energy of 350 GeV. This run produced 8300 charged current events. In 1980, 1981 and 1983 three more runs with a proton energy of 400 GeV took place, each one with a ratio of neutrino to antineutrino pictures of approximately 1:2. The target and the wide band beam set-up were kept identical. The 1980 and 1981 runs gave 5260 neutrino charged current events and 6520 antineutrino charged current events. The data samples presented here do not yet include the results of the 1983 run which is being processed.

The film was scanned twice for events with visible energy greater than 3 GeV. The scanning efficiency for 3-prong events was 95 ± 2%. The events were measured on 4 views on semi-automatic measuring devices in the different laboratories and geometrically reconstructed using the HYDRA geometry program. In a fiducial volume of 18.9 m^3 (containing 1.1 t of hydrogen) a minimum track length of 25 cm was required for non-stopping tracks. The precision of the measurements and of the geometrical reconstruction can be characterised by a r.m.s. residual of measured points with respect to the reconstructed trajectory of about 7μ on film.

High measurement precision is of great importance for the identification of reactions (1) and (2) amongst all 3-prong events. Firstly it helps in the identification of non-stopping protons by measuring the energy loss along the visible trajectory. 26% of all protons in reactions (1) and (2) stopped in the bubble chamber and another 18% could be identified by energy loss. Secondly the discriminative power of the kinematical fitting procedure against additional neutrals is greatly enhanced by particle identification and small track reconstruction errors.

The muons were identified by extrapolating the tracks of the non-interacting particles with momentum > 3 GeV/c outside the bubble chamber and by comparing them with hits in the External Muon Identifier (EMI) behind hadron absorbers. For the 1977 and 1980 runs the EMI consisted of 2 planes of MWPCs at 4.5 and 7 m, respectively, from the centre of the bubble chamber. For the 1981 run an Internal Picket Fence (IPF) of proportional tubes around the chamber body was added. The electronic efficiency of the EMI was ~ 98%. The geometrical acceptance varies from 40% at p(μ) = 3 GeV/c to 100% for p(μ) > 20 GeV/c. For the data sample considered here the EMI was operational for ~ 80% of the time.

The total sample of 3-prong events with EMI identification of the muon was passed through the HYDRA kinematical fitting program. All events were tested for the 3-constraint hypotheses of reactions (1), (2), (3) and (4). The χ^2 probability distributions, $P(\chi^2)$, of events fitting reactions (1) and (2) are shown in fig. 1. They are reasonably flat (as expected for a correct error treatment) but there is an excess of events at

probabilities < 2%. (Only events with $P(\chi^2) > 2\%$ are shown in fig. 1.) This excess is mainly due to contamination from events with additional neutral (unseen) particles. In the following analysis only events with $P(\chi^2) > 2\%$ and $E_\nu > 5$ GeV will be retained. About 95% of these fits are unique. Only 1% of events of reactions (1) and (3) have an ambiguity between p and π^+ or K^+; in these cases the fit with the larger probability was selected. In case of ambiguities between reactions (1) and (3) or reactions (2) and (4), the fit to the reaction with a pion was selected because reactions (1) and (2) are expected to be at least ten times more frequent than reactions (3) and (4) (see sect. 3.3). The event sample obtained under these conditions is summarised in Table 1 and it is studied in sect. 3.

To verify the efficiency of the fitting procedure, the remaining sample of 3-prong events was checked for approximate transverse momentum balance between the muon and the hadronic system. Only a small signal above background was found corresponding to 2% of the fitted sample. This loss has been corrected for in the absolute cross section calculation.

3. RESULTS

3.1 Production of ($p\pi$) systems with W < 2 GeV

In this section we shall study the properties of baryonic resonance production by the weak charged current. Most of the early theoretical work was concerned with $\Delta(1232)$ production both in reactions (1) and (2) and the data on Δ^{++} production were compared with models by several experiments [1-7], including ours. With our present data sample we can extend the study of resonances up to a mass of 2 GeV and compare in the same experiment the doubly charged ($p\pi^+$) system with I = 3/2 to the neutral ($p\pi^-$) system containing both I = 1/2 and 3/2 resonances. General production characteristics of the ($p\pi$) systems in the resonance regions in the two reactions are listed in Table 2.

The importance of the different isospin content becomes immediately apparent from the ($p\pi$) mass distributions shown in fig. 2. Reaction (1) is dominated by the production of $\Delta^{++}(1232)$ close to threshold. In the same channel we can now confirm a second accumulation of events at masses

between 1.6 and 2.0 GeV corresponding to at least five known I = 3/2 states with different spin-parities. The situation is more complex in reaction (2) where $\Delta^{\circ}(1232)$ production is clearly seen but it does not dominate the channel. The $(p\pi^-)$ system exhibits two more peaks at about 1.5 and 1.7 GeV and a gradual fall-off towards higher masses with a substantial cross section up to 2 GeV. The peak at 1.5 GeV can readily be explained by an important contribution from the N(1520) and N(1540) resonances and there are again many states, both with I = 1/2 and I = 3/2, which contribute to generate the accumulation between 1.6 and 2.0 GeV.

To account for the contributions of the different resonances, Rein and Sehgal [10] have generalised the relativistic harmonic oscillator model of Feynman, Kislinger and Ravndal [11] and its extension by Ravndal to the weak production of isolated resonances [12] by taking into account the amplitudes for their decays into $(N\pi)$ and by specifying the relative phases of the production amplitudes, thus allowing for their interference. Some non-resonant background was included in the I = 1/2 state without taking into account possible interference of this background with the resonances. Since there is little overlap of resonances of the same spin-parity, the effective mass distribution is only sensitive to the magnitude of their contribution and not to the phases. The curves shown in fig. 2 are the predictions of Rein and Sehgal, normalised to the number of events in reactions (1) and (2), respectively. The curves describe the shape of the mass distributions reasonably well.

Because of lack of statistics and the strong overlap of different resonances in reaction (2) we are not able to separate them and to determine their production cross sections. Instead, we present in fig. 3 the energy dependence of the production cross sections for all states with W < 2 GeV in reactions (1) and (2). The cross sections are calculated by comparing the number of events to the ν flux of the 1977 run and to the $\bar{\nu}$ flux of the 1980 run. These fluxes have been determined from the measured muon yields in the five gaps of the iron shielding of the neutrino beam line. The relation between the muon flux and the neutrino flux as a function of energy and distance to the beam axis in the bubble chamber is determined by a Monte-Carlo program [13] using the pion and kaon spectra in proton-proton collisions from the Thermodynamic Model

[14], adapted to the yields in p-Be collisions measured at 400 GeV. The neutrino and antineutrino fluxes can be determined by this technique to an accuracy better than 10% for all neutrino energies above 10 GeV. The cross sections are compatible with being constant for neutrino energies above 20 GeV as predicted by all models. For E_ν between 10 and 80 GeV and for $W < 2$ GeV, we find average cross sections of $(68 \pm 7)\ 10^{-40}$ cm^2 for reaction (1) and $(30 \pm 4)\ 10^{-40}$ cm^2 for reaction (2). The curves in fig. 3 show the predictions by Rein and Sehgal.

The distributions in Q^2 (the negative value of the lepton 4-momentum transfer squared) are plotted in fig. 4 for two mass intervals of reactions (1) and (2). The cross section falls off rather steeply with Q^2 at low ($p\pi$) masses ($1.1 < W < 1.4$ GeV). This fall-off becomes less steep for higher mass states ($1.4 < W < 2$ GeV). At fixed W the fall-off is of comparable size in the ν and $\bar{\nu}$ reactions. The Q^2 distributions at low W are fairly well described by the Rein-Sehgal model. However, in the $\bar{\nu}$ reaction a dip is observed for $Q^2 < 0.1$ GeV^2 in both mass intervals. We have verified that this dip is not caused by experimental losses. Our data, therefore, confirm this dip at small Q^2 which there were indications for in previous data [8,9]. There are no theoretical predictions either for the dip or for the change of slope of the Q^2 distribution with increasing W.

Angular distributions of the hadrons in the ($p\pi$) rest frame are sensitive to production mechanisms and interferences of different partial wave amplitudes. We choose the pion as analyser and measure its direction angles θ_π and ϕ_π in the ($p\pi$) rest frame in the reference frame shown in fig. 5. The polar angle is measured with respect to the lepton momentum transfer vector $\vec{Q} = \vec{P}_\nu - \vec{P}_\mu$ and the azimuthal angle ϕ_π is measured around $\vec{Q}$. The axis $\phi_\pi = 0$ is defined as the projection of the muon momentum vector $\vec{P}_\mu$ onto a plane perpendicular to $\vec{Q}$. Fig. 6 shows the two-dimensional plot of $\cos\theta$ versus W, the effective mass of the ($p\pi$) system. For $W < 2$ GeV the full $\cos\theta_\pi$ range is populated, as expected for a single resonance or the overlap of a few resonances. Near $W = 2$ GeV a peak develops at $\cos\theta = 1$ and becomes very pronounced at high W (see also figs 10(b) and 10(e)). This indicates that a peripheral production mechanism of pions is replacing resonance production as the dominating

process at large values of W (see sect. 3.2). The distributions of the azimuthal angle ϕ_π for events with W < 2 GeV are flat. These distributions are not shown but the values of $\langle\cos\phi_\pi\rangle$ and $\langle\sin\phi_\pi\rangle$ are presented in Table 2.

For comparison of angular distributions with models it is convenient to expand the distribution into spherical harmonics:

$$N(\theta,\phi) = \sum_{l,m} a_{lm} Y_l^m(\theta,\phi). \qquad (5)$$

In fig. 7 we compare moments $a_{lm} = \langle Y_l^m(\theta,\phi)\rangle$ with predictions of the Rein-Sehgal model for reaction (2) for W values from threshold up to 1.6 GeV. Despite the large errors, the data appear to be incompatible with the predictions. With the present statistics the data do not allow a more detailed investigation to find the reasons for this disagreement. (The dashed curves in fig. 7 are the results of the Rein-Sehgal model with the phase of the resonance P_{11} (1450) taken with the sign opposite to that used in the Feynman-Kislinger-Ravndal model.)

3.2 Production of (pπ) systems with W > 2 GeV

Fig. 8 shows the cross sections for reactions (1) and (2) as functions of the (anti) neutrino energy, integrated over all W > 2 GeV. These cross sections have been determined as explained in sect. 3.1. The average values of the cross sections shown in fig. 8 are (9.4 ± 1.4) 10^{-40} cm^2 for reaction (1) and (12 ± 2) 10^{-40} cm^2 for reaction (2), both in the energy range 10-80 GeV. The ratio of the cross sections of reaction (1) to the cross section of reaction (2) is 0.78 ± 0.18, i.e. the cross sections for producing a high mass (pπ) system are similar in the two reactions and compatible with being equal.

We have studied many kinematic variables for these reactions, including those normally used for the description of deep inelastic reactions. Fig. 9 shows the distributions of Q^2 and z_π. The Q^2 distributions of the two reactions at high W are wider than at low W. This continues the trend of growing $\langle Q^2\rangle$ with increasing W already observed in the resonance region (sect. 3.1). Remembering that z_π is the fraction of the current energy carried by the pion

$$z_\pi = \frac{E_\pi}{E_\nu - E_\mu} \quad ,$$

we notice that both in reactions (1) and (2) the pion takes essentially all the current energy. (The particle energies in the laboratory frame have been used to calculate z_π.) The average value of z_π is 0.9 in both reactions. This can be compared with $\langle z_\pi \rangle = 0.6$ for the low W reactions. The fact that the proton behaves like a spectator particle in the high W reactions is also apparent in the scatter plots shown in fig. 6 and in the $\cos\theta_\pi$ distributions shown in figs 10(b) and 10(e).

A comparison of the global features of the high mass part of reactions (1) and (2) is presented in Table 3. A near equality of the differential distributions expressed through the averages is apparent.

The data suggest that the dominant diagram for the production of high mass ($p\pi$) systems in reactions (1) and (2) is

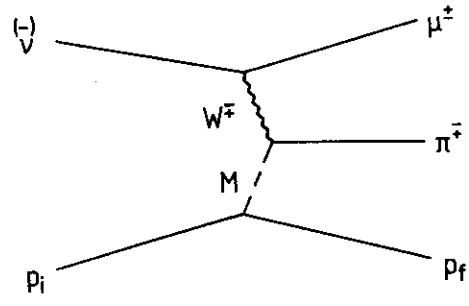

where W is the Intermediate Vector Boson, p_i and p_f are the initial and final state protons and M is a virtual meson state. Other particles are represented by their usual symbols. If the exchanged neutral meson M has definite G-parity (implying the absence of V-A interference) we expect the cross sections for reactions (1) and (2) to be equal. The data show that they are equal within errors. The following analysis does not assume that M is a single meson state. However, we find evidence that one state dominates.

The distribution of the variable t, the negative value of the 4-momentum transfer squared to the proton,

$$t = -(p_f - p_i)^2$$

is shown in fig. 10(a) and (d). The distributions are not as peaked as one would naively expect for pion exchange (i.e. M = π^o). However, a simple Regge pole description shows that the data are consistent with π^o-exchange. An explanation of this analysis follows.

The differential cross section for reactions (1) and (2) can be parametrized in the following model-independent way:

$$\frac{d^3\sigma}{dQ^2dW^2dt} = \Gamma(E_\nu, Q^2, W^2) \cdot \frac{d\sigma}{dt}(Q^2, W^2, t) \qquad (6)$$

where Γ is the flux factor of the virtual Weak Vector Boson and $d\sigma/dt$ is the differential cross section for its interaction with the proton leading to a final state of effective mass W at fixed Q^2 and t. The expression for Γ is given explicitly by Bartl et al. [15]. If the virtual meson M in the diagram is described by a Regge pole, then we can express the differential cross section as

$$\frac{d\sigma}{dt} \sim \beta(t,Q^2)s^{2[\alpha(t)-1]} = \beta(t,Q^2)s^{2(\alpha_o-1)}\, e^{-(2\alpha'\ln s)t} \qquad (7)$$

where $s = W^2$ and the Regge trajectory is $\alpha(t) = \alpha_o - \alpha' t$. The constants α_o and α' are, respectively, the intercept and the slope of the Regge trajectory on a Chew-Frautschi plot. The presence in (7) of a poorly known vertex function $\beta(t,Q^2)$ makes it practically impossible to predict the t-dependence of the hadronic distribution. However, for any chosen value of the intercept α_o one obtains a prediction for the W^2 dependence of the cross section. For such a prediction the shape of the energy distribution of the (anti)neutrino beam in our experiment has to be included in the calculation of the flux factor Γ.

In order to analyse the W^2 distribution of the data in terms of Regge exchanges, we combine the data of reactions (1) and (2) to get better statistics. The W^2 distribution is shown in fig. 11. The curves shown are normalised to the total number of events and correspond to pion exchange ($\alpha_o = 0$), vector meson exchange (ρ^o, ω^o; $\alpha_o = 0.5$) and Pomeron exchange ($\alpha_o = 1$). The data clearly exclude Pomeron exchange and are compatible with pure pion exchange; some contribution of vector meson exchange cannot be excluded, however.

A qualitative prediction of the Regge model for the t-distribution is that $d\sigma/dt$ should fall off faster with t at high W^2 than at low W^2. Fig. 12 shows the t-distribution for the combined data of reactions (1) and (2) (a) for $4 < W^2 < 8$ GeV^2 and (b) for $W^2 > 8$ GeV^2. The slope parameters B in the fitted distributions of the form $A \exp(-B \cdot t)$ are $B = 1.7 \pm 0.2$ GeV^{-2} for the lower W^2 bin and $B = 3.5 \pm 0.5$ GeV^{-2} for $W^2 > 8$ GeV^2 in agreement with the qualitative predictions of the Regge model.

We have also looked for a possible correlation between the orientation of the leptonic plane and the plane formed by the incoming and outgoing protons as seen in the $\mu\pi$ rest system (Treiman-Yang test). We find no correlation, which is consistent with the assumption that M is spinless.

Finally we will discuss the distribution of the azimuthal angle of the pion, ϕ_π. This angle has been defined in the previous chapter (fig. 5) and its distribution is shown in figs 10(c) and (f). The V-A nature of the weak charged current implies that the most general expression for the ϕ_π distribution can be written as

$$\frac{d\sigma}{d\phi_\pi} = a + b\cos\phi_\pi + c\cos2\phi_\pi + d\sin\phi_\pi + e\sin2\phi_\pi \qquad (8)$$

where the coefficients a to e are functions of the cross sections for different polarisation states of the Intermediate Vector Boson and of other kinematic variables [15]. Table 3 lists the average values $\langle\cos\phi_\pi\rangle$, $\langle\cos2\phi_\pi\rangle$, $\langle\sin\phi_\pi\rangle$ and $\langle\sin2\phi_\pi\rangle$ which are proportional to the coefficients b, c, d and e. They are all compatible with zero except coefficient b. It is interesting that $\langle\cos\phi_\pi\rangle$ has the same value (within errors) and the same sign in the two reactions. This means that there is little or no V-A interference in the $\cos\phi$ term in (8). In fig. 13 we plot the distribution of $\cos\phi_\pi$ for the combined sample of reactions (1) and (2) for $W > 2$ GeV. We find $\langle\cos\phi_\pi\rangle = 0.19 \pm 0.05$.

A non-zero value of $\langle\cos\phi_\pi\rangle$ has never been observed in an exclusive neutrino reaction before. A detailed interpretation of eq. (8) shows that a non-vanishing value of $\langle\cos\phi_\pi\rangle$ originates from an interference of a Intermediate Vector Boson amplitude of longitudinal polarisation with those of transverse polarisation. Therefore, we have established the

contribution of longitudinally polarised Intermediate Vector Bosons to this exclusive reaction. This is in contrast to deep inelastic inclusive neutrino reactions where the contribution of states of longitudinal polarisation has been measured to be very small. On the other hand, a similar polarisation effect has been observed in some low energy electroproduction reactions [16].

The parity-violating terms $\sin\phi_\pi$ and $\sin 2\phi_\pi$ are T-odd. Thus their average values can be non-zero only in the presence of final state hadron interactions. If there is only one dominant Regge pole exchange, the phases of all hadronic amplitudes will be equal and then coefficients d and e are expected to vanish.

3.3 Production of (pK) systems

In (anti)neutrino interactions on protons the production of single strange particles is possible via the flavour-changing charged current interactions (3) and (4) which on the quark level read as

$$\nu\bar{u}(u) \rightarrow \mu^- \bar{s}(u) \qquad (9)$$

$$\nu s(\bar{s}) \rightarrow \mu^- u(\bar{s})$$

and

$$\bar{\nu} u \rightarrow \mu^+ s \qquad (10)$$

$$\bar{\nu} s(s) \rightarrow \mu^+ \bar{u}(s)$$

which are all Cabbibo-suppressed. Therefore, the rates for single kaon production (reactions (3) and (4)) are expected to be smaller than those for reactions (1) and (2) by at least one order of magnitude. Furthermore, since the neutrino reactions (9) can only take place on sea quarks, kaon production is expected to be still smaller in νp than in $\bar{\nu} p$ interactions.

Experimentally it is much more difficult to select clean and complete samples of reactions (3) and (4) than of reactions (1) or (2). These difficulties arise from the following facts: Firstly, at increasing laboratory momentum of the meson, the discriminative power of the kinematic fit becomes less and less sensitive to the mass difference between kaons and pions. Therefore, fits tend to become ambiguous between

reactions (1) and (3) and between (2) and (4), respectively. Because of the much higher rate of reactions (1) and (2) we have ignored ambiguous fits to reactions (3) and (4) and we are left with unique fits only which are biased towards lower laboratory momentum of the kaon. Secondly, even unique fits of reactions (3) and (4) may contain background from the reactions

$$\overset{(-)}{\nu}p \rightarrow \mu^{\pm} p \pi^{\mp} \pi^{o}$$

which again have a much higher cross section. If the π^o in these reactions has negligible transverse momentum with respect to the beam direction and an appropriate longitudinal momentum a fit to reactions (3) or (4) may result by replacing the $(\pi^{\mp}\pi^{o})$ system by a fake kaon. However, these fake fits should cluster at low probabilities of the kinematic fit.

We have obtained 41 unique fits to reactions (3) and 40 to reaction (4) the probability distributions of which are shown in fig. 14. There is indeed an accumulation of fits at low probabilities which we eliminate by selecting events with $P(\chi^2) > 2\%$, leaving 26 and 31 events assigned to reactions (3) and (4), respectively. From an investigation of the momentum distribution of mesons in 3-prong charged current events with missing neutrals we estimate the background remaining after the probability cut to be of 1 to 2 events in each of the two channels.

The effective mass distributions of the (pK) systems in reactions (3) and (4) are shown in fig. 15. No particular structure can be seen in the (pK^+) distribution whereas some accumulation of events around W = 1.5 GeV is observed in the (pK^-) mass distribution of reaction (4). We interpret this accumulation as production of the $\Lambda(1520)$ resonance, as such clustering is unlikely to be produced by background events. We estimate 5 ± 3 events to come from this resonance resulting in a cross section of (2.8 ± 2.1) 10^{-40} cm^2 for the production of $\Lambda(1520)$ (using the decay branching ratio of 23% for $\Lambda(1520)$ into pK^-). The value found may indicate a cross section somewhat larger than $0.5\ 10^{-40}$ cm^2 - an estimate for the cross section by Finjord and Ravndal [17], based on a relativistic quark model.

4. CONCLUSIONS

We have investigated exclusive single charged meson production in high energy neutrino and antineutrino interactions on protons in the reactions $\nu p \to \mu^- p\pi^+$, $\bar{\nu}p \to \mu^+ p\pi^-$, $\nu p \to \mu^- pK^+$ and $\bar{\nu}p \to \mu^+ pK^-$.

In single pion production we can clearly distinguish two production mechanisms. At low effective mass of the $(p\pi)$ system the pions are decay products of baryonic resonances excited by the weak charged current. The relative contribution of these resonances, their absolute production cross section, Q^2 distributions and angular distributions have been predicted in different quark models. The cross sections of $(68 \pm 7)\ 10^{-40}$ cm^2 for $(p\pi)$ systems with $W < 2$ GeV in νp interactions and of $(30 \pm 4)\ 10^{-40}$ cm^2 in $\bar{\nu}p$ interactions found in our experiment agree reasonably well with the predictions. However, there is definite disagreement with the Rein-Sehgal model in the decay angular distributions of the $(p\pi)$ systems in $\bar{\nu}p$ interactions.

For effective masses of the $(p\pi)$ system larger than 2 GeV the angular distribution of the pion becomes more and more peaked into the direction of the weak current. This transition from resonance production to a peripheral production mechanism is very similar to the same phenomenon in hadronic interactions where the peripheral nature of the interaction has been explained by the exchange of a virtual particle between projectile and target. Studying momentum transfer distributions to the proton and the dependence of the production cross section on the effective mass of the $(p\pi)$ system we find evidence for the weak interaction taking place on a virtual π^o. There is no evidence for diffractive production of single pions. This is not surprising as at our neutrino energies there is little cross section for $W > 10$ GeV where diffractive mechanisms start to set in. Investigating the azimuthal distribution of pions around the direction of the weak current we find an asymmetry which must be due to contributions from longitudinally polarised Weak Vector Bosons. We are not aware of any theoretical prediction for this process.

We also observe single kaon production in νp and $\bar{\nu}p$ interactions which in the Cabbibo theory is caused by flavour-changing charged currents.

Because of experimental limitations we can only establish low momentum (pK) systems which - as in single pion production - seem to contain resonance production. We observe the production of Λ(1520) with a cross section of $(2.8 \pm 2.1)\ 10^{-40}\ cm^2$. This value is somewhat larger than quark model estimates taking into account the Cabbibo suppression factor $\sin^2\theta_c$.

We would like to thank Drs Rein and Sehgal for numerous discussions on weak resonance production and for providing us with calculations matched to our experimental conditions. We also thank Dr. Majerotto for discussions on peripheral pion production. We want to acknowledge the excellent work of the CERN staff operating BEBC, the EMI and the neutrino beam. Finally we thank the scanning, measuring and computing staff of our laboratories for their diligent work.

REFERENCES

[1] I. Bugadov et al., Phys. Lett. 29B (1969) 524.

[2] W. Lerche et al., Phys. Lett. 78B (1978) 510.

[3] N.J. Baker et al., Phys. Rev. D23 (1981) 2495.

[4] G.M. Radecky et al., Phys. Rev. D25 (1982) 1161.

[5] J. Bell et al., Phys. Rev. Lett. 41 (1978) 1008; 1012.

[6] P. Allen et al., Nucl. Phys. B176 (1979) 269.

[7] T. Bolognese et al., Phys. Lett. 81B (1979) 393.

[8] S.J. Barish et al., Phys. Lett 91B (1980) 161.

[9] D. Allasia et al., Zeitschrift f.Phys. C20 (1983) 95.

[10] D. Rein and L.M. Sehgal, Ann. of Phys. 133 (1981) 79.

[11] R.P. Feynman, M. Kislinger and F. Ravndal, Phys. Rev. D3 (1971) 2706.

[12] F. Ravndal, Nuovo Cimento Lett. 3 (1972) 631 and 18A (1973) 385.

[13] W. Venus and H. Wachsmuth, CERN Int.Rep. CERN/EP/NBU 79-1.

[14] R. Hagedorn and J. Ranft, Nucl. Phys. B48 (1972) 15.

[15] A. Bartl et al., Phys. Rev. D16 (1977) 2124.

[16] D.R. Botterill et al., Nucl. Phys. B116 (1976) 65;
A. del Guerra et al., Nucl.Phys. B107 (1976) 65;
C.J. Bebek et al., Phys. Rev. D9 (1974) 1229;
C.J. Bebek et al., Phys. Rev. D13 (1976) 25.

[17] J. Finjord and F. Ravndal, Nucl. Phys. B106 (1976) 228.

TABLE CAPTIONS

TABLE 1 Data sample.

TABLE 2 Averages of kinematical quantities and cross sections for $W(p\pi) < 2$ GeV.

TABLE 3 Averages of kinematical quantities and cross sections for $W(p\pi) > 2$ GeV.

TABLE 1

Reaction	Selection criteria	No. of events W < 2 GeV	W > 2 GeV	Total
$\nu p \to \mu^- + X$	Muon identified by			13560
$\bar{\nu} p \to \mu^+ + X$	EMI, $p_\mu > 3$ GeV/c			6520
$\nu p \to \mu^- p \pi^+$	As above and kinematic	1027	128	1155
$\bar{\nu} p \to \mu^+ p \pi^-$	fit $P(\chi^2) > 2\%$	278	97	375
$\nu p \to \mu^- p K^+$	As above and fit unique	11	15	26
$\bar{\nu} p \to \mu^+ p K^-$		19	12	31

TABLE 2

	$\nu p \to \mu^- p \pi^+$	$\bar{\nu} p \to \mu^+ p \pi^-$
$\langle E_\nu \rangle$, GeV	24.8	25.9
$\langle \nu = E_\nu - E_\mu \rangle$, GeV	0.9	1.4
$\langle p_{lab}(\pi) \rangle$, GeV	0.48	0.8
$\langle Q^2 \rangle$, GeV^2	0.78 ± 0.04	1.26 ± 0.09
$\langle t \rangle$, GeV^2	0.72 ± 0.02	1.04 ± 0.06
$\langle \cos\theta_\pi \rangle$	0.10 ± 0.04	0.24 ± 0.03
$\langle \cos\phi_\pi \rangle$	0.04 ± 0.02	0.02 ± 0.04
$\langle \sin\phi_\pi \rangle$	0.06 ± 0.02	0.02 ± 0.04
$\langle z_\pi \rangle$	0.60 ± 0.01	0.63 ± 0.01
$\langle \sigma \rangle$, 10^{-40} cm^2	68 ± 7	30 ± 4

TABLE 3

	$\nu p \to \mu^- p\pi^+$	$\bar{\nu} p \to \mu^+ p\pi^-$
$\langle E_\nu \rangle$, GeV	32.6	32.0
$\langle \nu = E_\nu - E_\mu \rangle$, GeV	6.4	6.4
$\langle p_{lab}(\pi) \rangle$, GeV	4.3	4.9
$\langle W(p\pi) \rangle$, GeV	2.9	3.0
$\langle Q^2 \rangle$, GeV^2	1.6 ± 0.2	2.3 ± 0.3
$\langle t \rangle$, GeV^2	0.70 ± 0.10	0.54 ± 0.07
$\langle \cos\theta_\pi \rangle$	0.77 ± 0.04	0.87 ± 0.02
$\langle \cos\phi_\pi \rangle$	0.20 ± 0.06	0.18 ± 0.07
$\langle \sin\phi_\pi \rangle$	0.10 ± 0.06	0.02 ± 0.07
$\langle \cos 2\phi_\pi \rangle$	0.05 ± 0.06	-0.11 ± 0.07
$\langle \sin 2\phi_\pi \rangle$	-0.08 ± 0.06	0.02 ± 0.07
$\langle z_\pi \rangle$	0.89 ± 0.02	0.93 ± 0.01
$\langle \sigma \rangle$, 10^{-40} cm^2	9.4 ± 1.4	12 ± 2

FIGURE CAPTIONS

Fig. 1 χ^2 probability distribution of kinematic fits (a) from reaction (1) and (b) from reaction (2).

Fig. 2 Effective mass distributions (a) $W(p\pi^+)$ for reaction (1) and (b) $W(p\pi^-)$ for reaction (2). The curves are predictions by Rein and Sehgal [10].

Fig. 3 Cross sections for production of $(p\pi)$ states with effective mass $W < 2$ GeV as functions of the incident (anti)neutrino energy, (a) in reaction (1) and (b) in reaction (2).

Fig. 4 Distributions of Q^2 for two subregions of $W(p\pi)$: $W < 1.4$ GeV (plots (a) and (b)) and $1.4 < W < 2.0$ GeV (plots (c) and (d)). Plots (a) and (c) show data of reaction (1), (b) and (d) of reaction (2).

Fig. 5 Definition of the pion direction angles θ_π and ϕ_π in the $(p\pi)$ restframe .

Fig. 6 Scatter plots: (a) $W(p\pi^+)$ versus $\cos\theta_\pi$ for reaction (1) and (b) $W(p\pi^-)$ versus $\cos\theta_\pi$ for reaction (2).

Fig. 7 Plots of the measured moments $\langle Y_1^m \rangle$, defined in eq. (5), for reaction (2). Curves are predictions of the Rein-Sehgal model (see text and ref. [10]).

Fig. 8 Cross sections for production of $(p\pi)$ systems with mass $W > 2$ GeV, (a) in reaction (1) and (b) in reaction (2).

Fig. 9 Distribution of Q^2 and z_π for events with $W > 2$ GeV for reaction (1) (plots (a) and (b)) and for reaction (2) (plots (c) and (d)).

Fig. 10 Distributions of variables t, $\cos\theta_\pi$ and ϕ_π for events with $W > 2$ GeV for reaction (1) (plots (a), (b), (c)) and for reaction (2) (plots (d), (e), (f)).

FIGURE CAPTIONS (Cont'd)

Fig. 11 Distribution of W^2 for the combined samples of reactions (1) and (2) with $W > 2.0$ GeV, with no cuts on other variables. Curves are from a Regge model calculation described in the text.

Fig. 12 Distribution of $|t|$ for the combined samples of reactions (1) and (2) for events (a) with $4 < W^2 < 8$ GeV^2 and (b) with $W^2 > 8$ GeV. The straight lines on these logarithmic plots are exponential fits to the data .

Fig. 13 Distribution of the azimuthal angle ϕ_π of pions in the combined sample of events of reactions (1) and (2) with $W > 2.0$ GeV.

Fig. 14 χ^2 probability distribution of unique kinematic fits (a) to reaction (3) and (b) to reaction (4).

Fig. 15 Effective mass distributions (a) $W(pK^+)$ for reaction (3) and (b) $W(pK^-)$ for reaction (4).

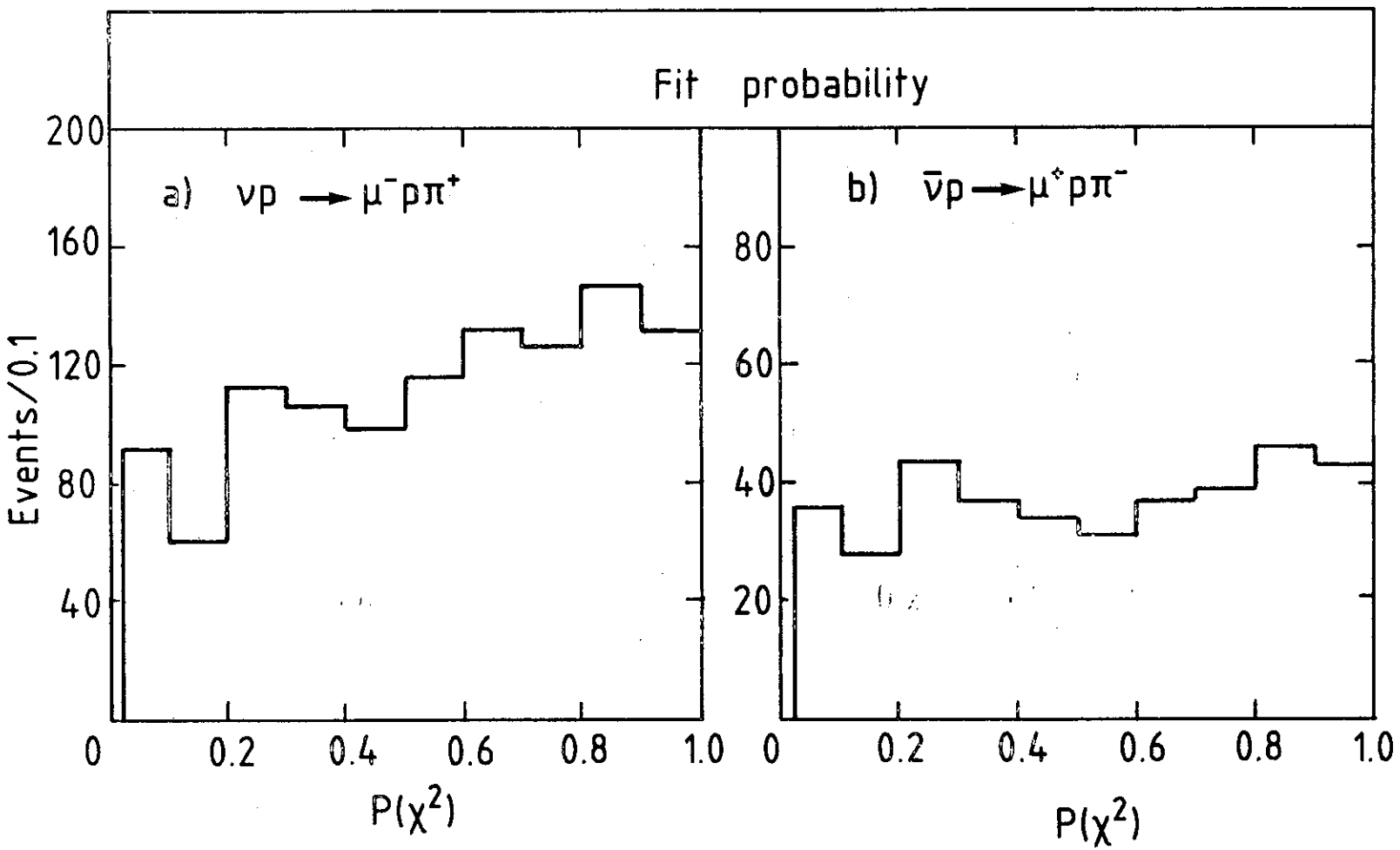
Fit probability
a) νp → μ⁻pπ⁺
b) ν̄p → μ⁺pπ⁻
Events/0.1
200
160
120
80
40
80
60
40
20
0
0.2
0.4
0.6
0.8
1.0
P(χ²)
P(χ²)

Fig. 1

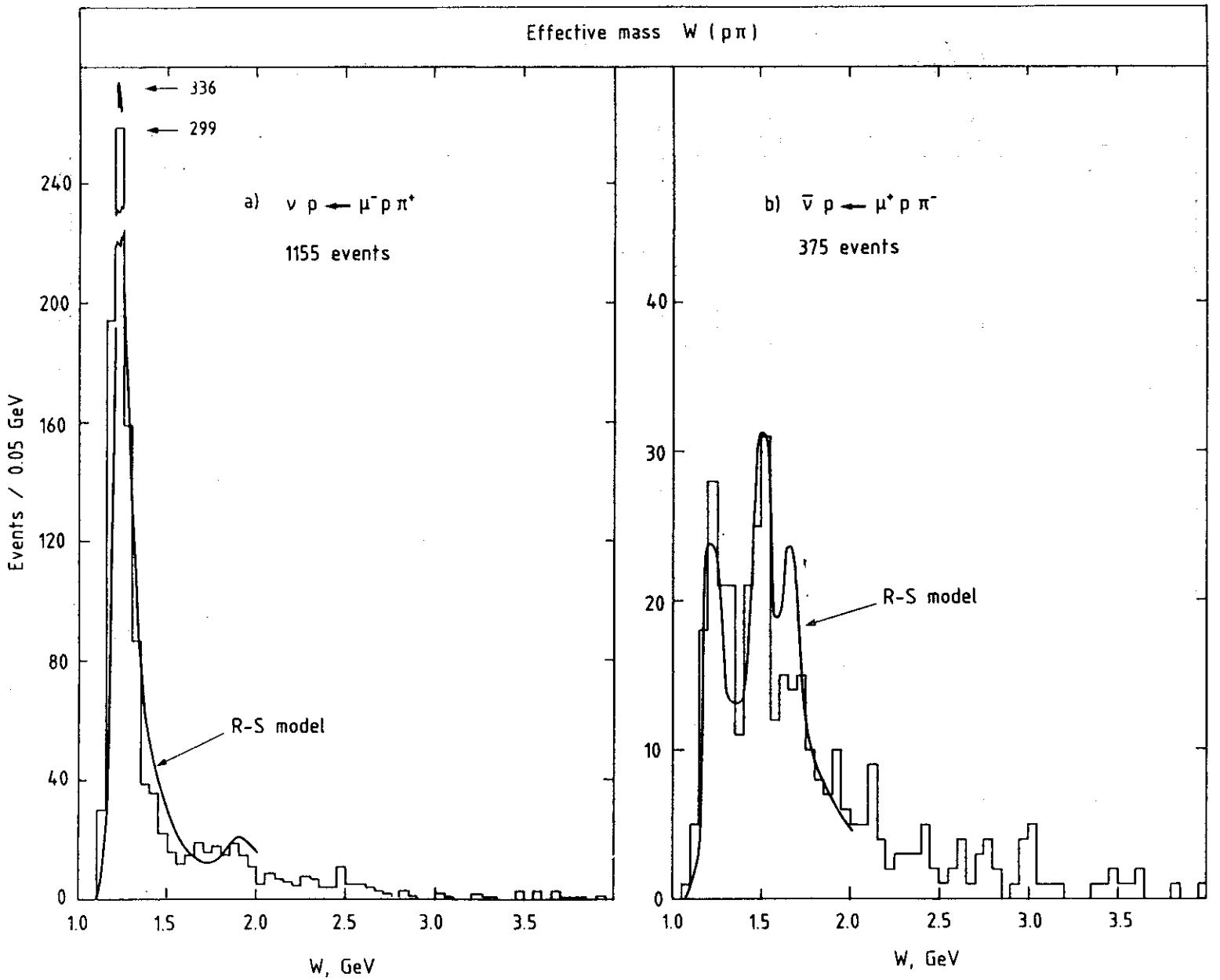
Effective mass W (pπ)
336
299
a) ν p ← μ⁻ p π⁺
1155 events
b) ν̄ p ← μ⁺ p π⁻
375 events
R-S model
R-S model
Events / 0.05 GeV
W, GeV
W, GeV

Fig. 2

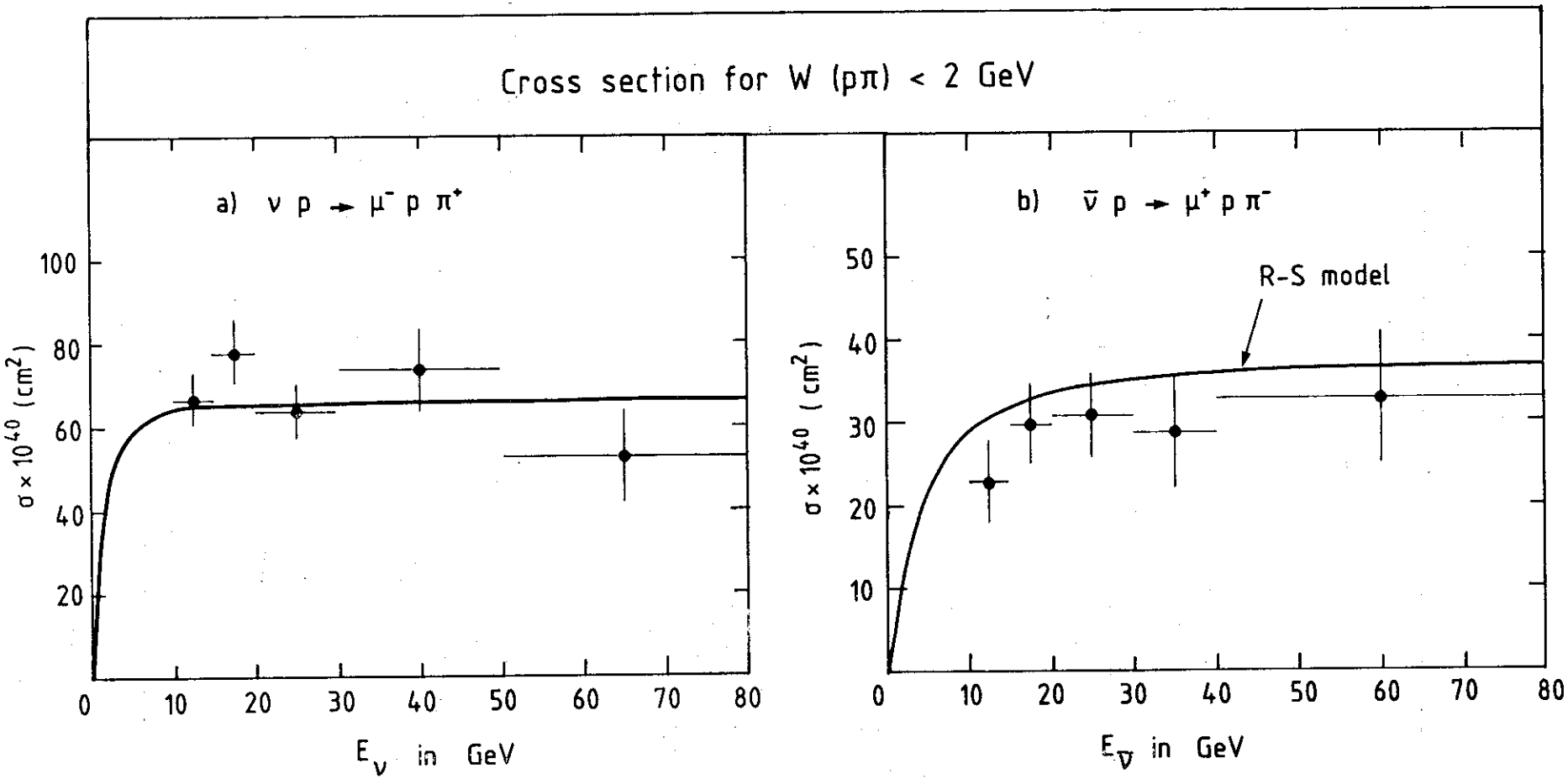
Cross section for W (pπ) < 2 GeV
a) ν p → μ⁻ p π⁺
b) ν̄ p → μ⁺ p π⁻
R-S model
σ × 10⁴⁰ (cm²)
E_ν in GeV
E_ν̄ in GeV

Fig. 3

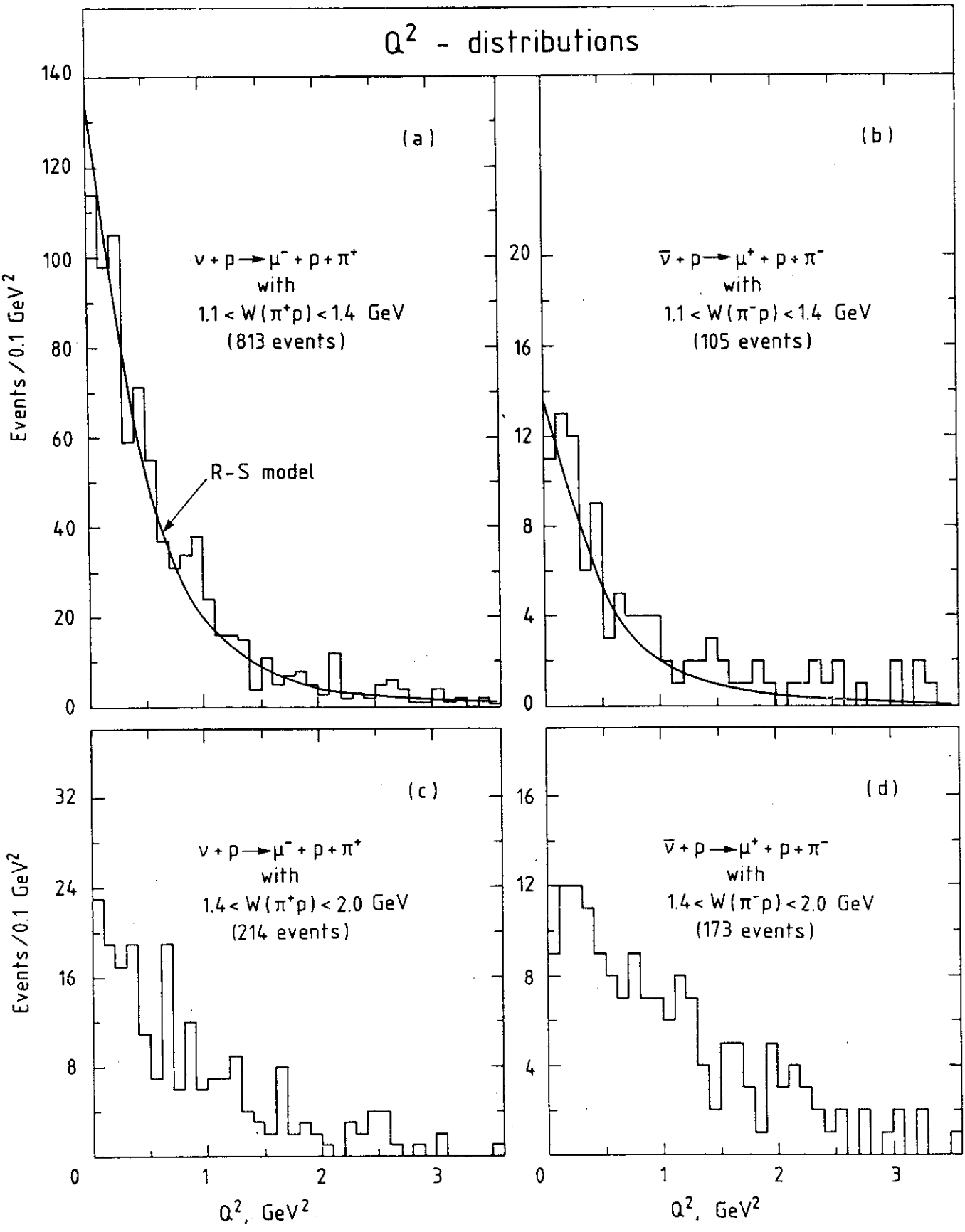
Q^2 - distributions
(a)
$\nu + p \rightarrow \mu^- + p + \pi^+$
with
$1.1 < W(\pi^+ p) < 1.4$ GeV
(813 events)
R-S model
(b)
$\bar{\nu} + p \rightarrow \mu^+ + p + \pi^-$
with
$1.1 < W(\pi^- p) < 1.4$ GeV
(105 events)
(c)
$\nu + p \rightarrow \mu^- + p + \pi^+$
with
$1.4 < W(\pi^+ p) < 2.0$ GeV
(214 events)
(d)
$\bar{\nu} + p \rightarrow \mu^+ + p + \pi^-$
with
$1.4 < W(\pi^- p) < 2.0$ GeV
(173 events)
Events / 0.1 GeV^2
Events / 0.1 GeV^2
Q^2, GeV^2
Q^2, GeV^2

Fig. 4

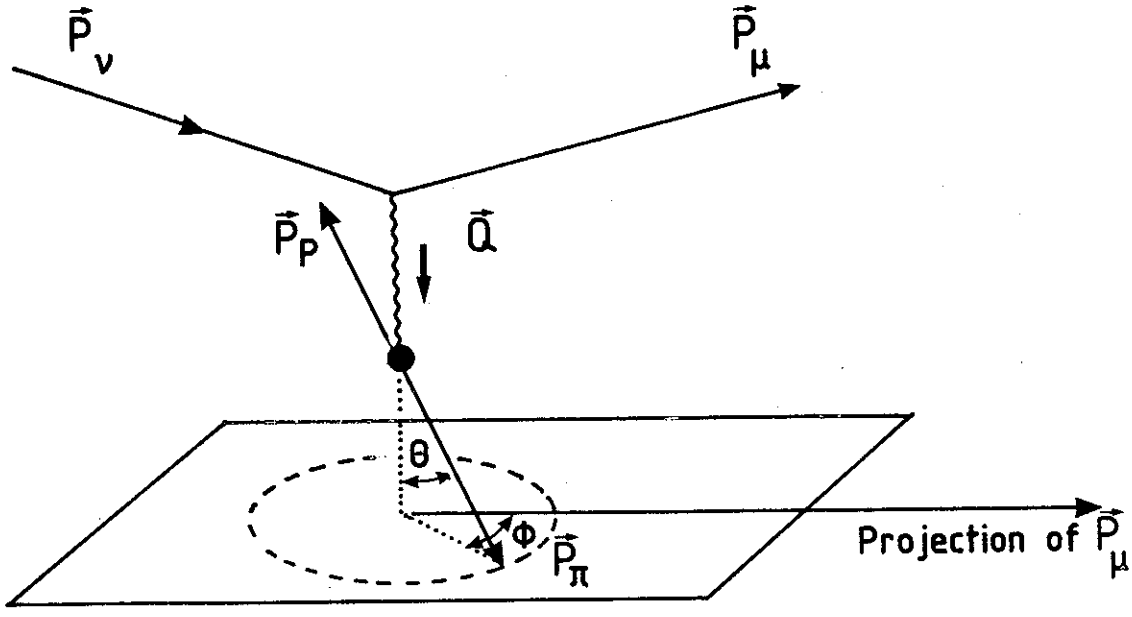

Fig. 5

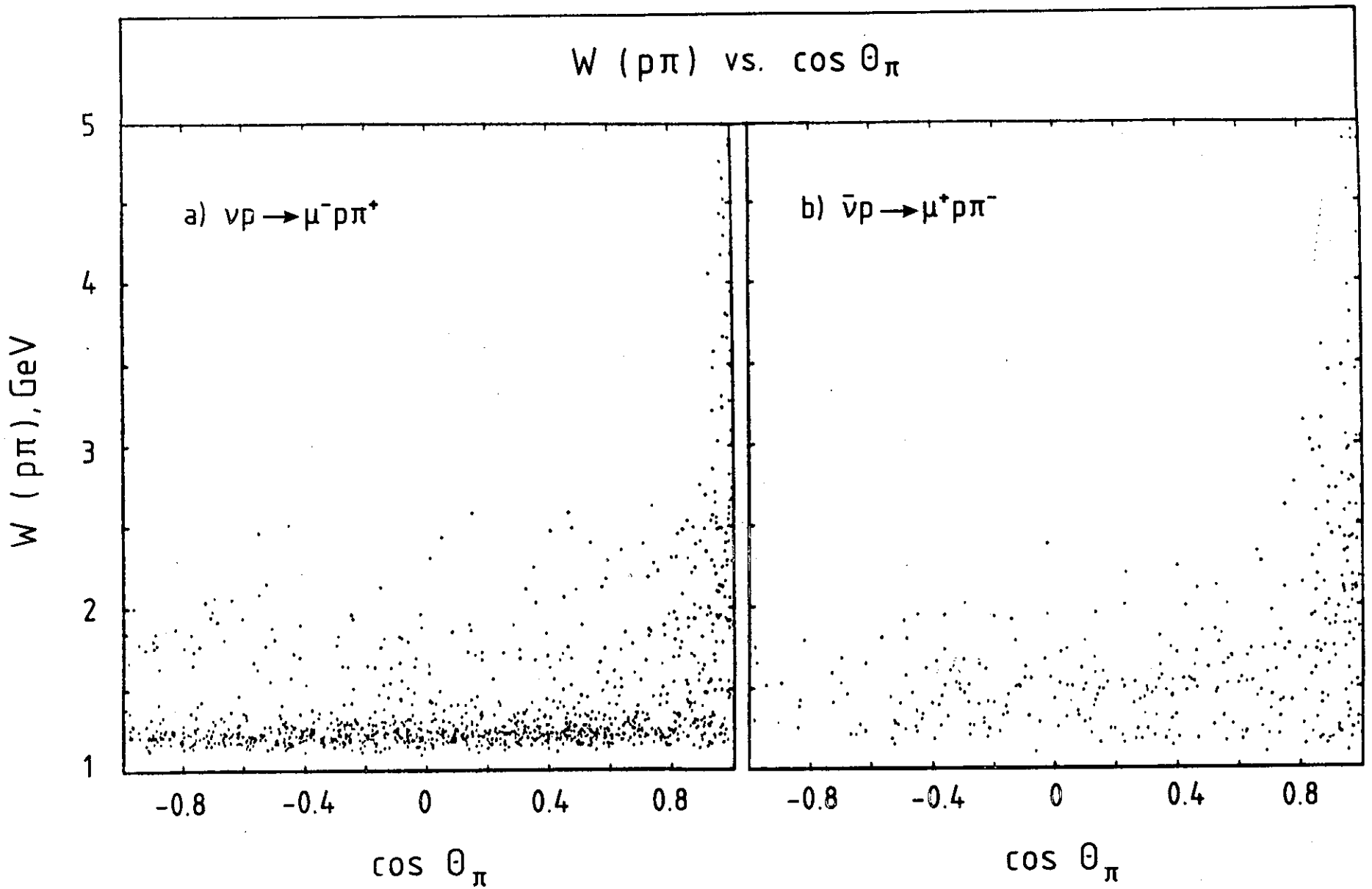
W (pπ) vs. cos θπ
a) νp → μ⁻pπ⁺
b) ν̄p → μ⁺pπ⁻
W (pπ), GeV
5
4
3
2
1
-0.8
-0.4
0
0.4
0.8
cos θπ
cos θπ

Fig. 6

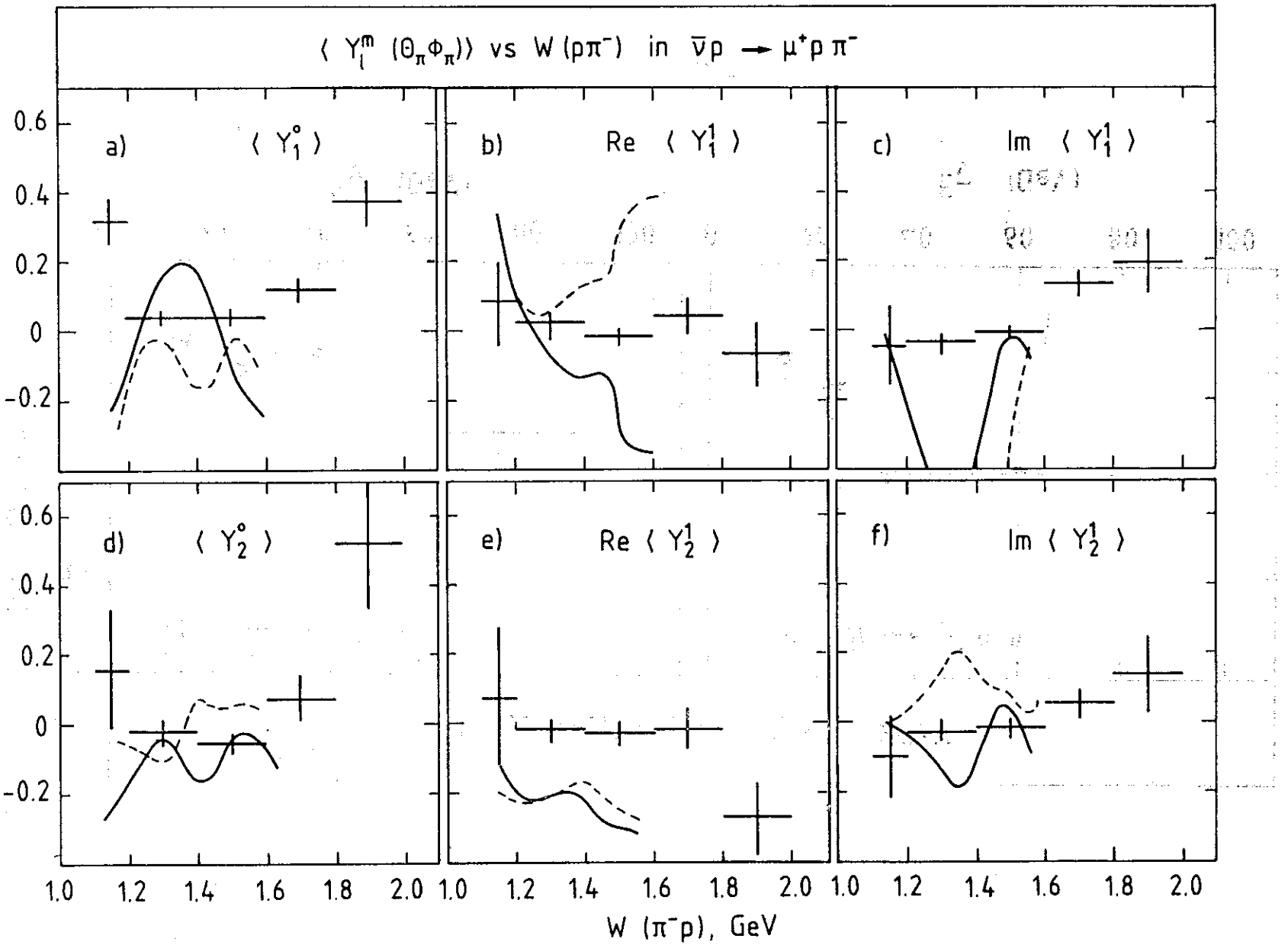
⟨ Y_l^m $(\Theta_\pi \Phi_\pi)$⟩ vs W $(p\pi^-)$ in $\bar{\nu}p \rightarrow \mu^+ p \pi^-$
a) ⟨ Y_1^0 ⟩
b) Re ⟨ Y_1^1 ⟩
c) Im ⟨ Y_1^1 ⟩
d) ⟨ Y_2^0 ⟩
e) Re ⟨ Y_2^1 ⟩
f) Im ⟨ Y_2^1 ⟩
0.6
0.4
0.2
0
-0.2
1.0
1.2
1.4
1.6
1.8
2.0
W $(\pi^- p)$, GeV

Fig. 7

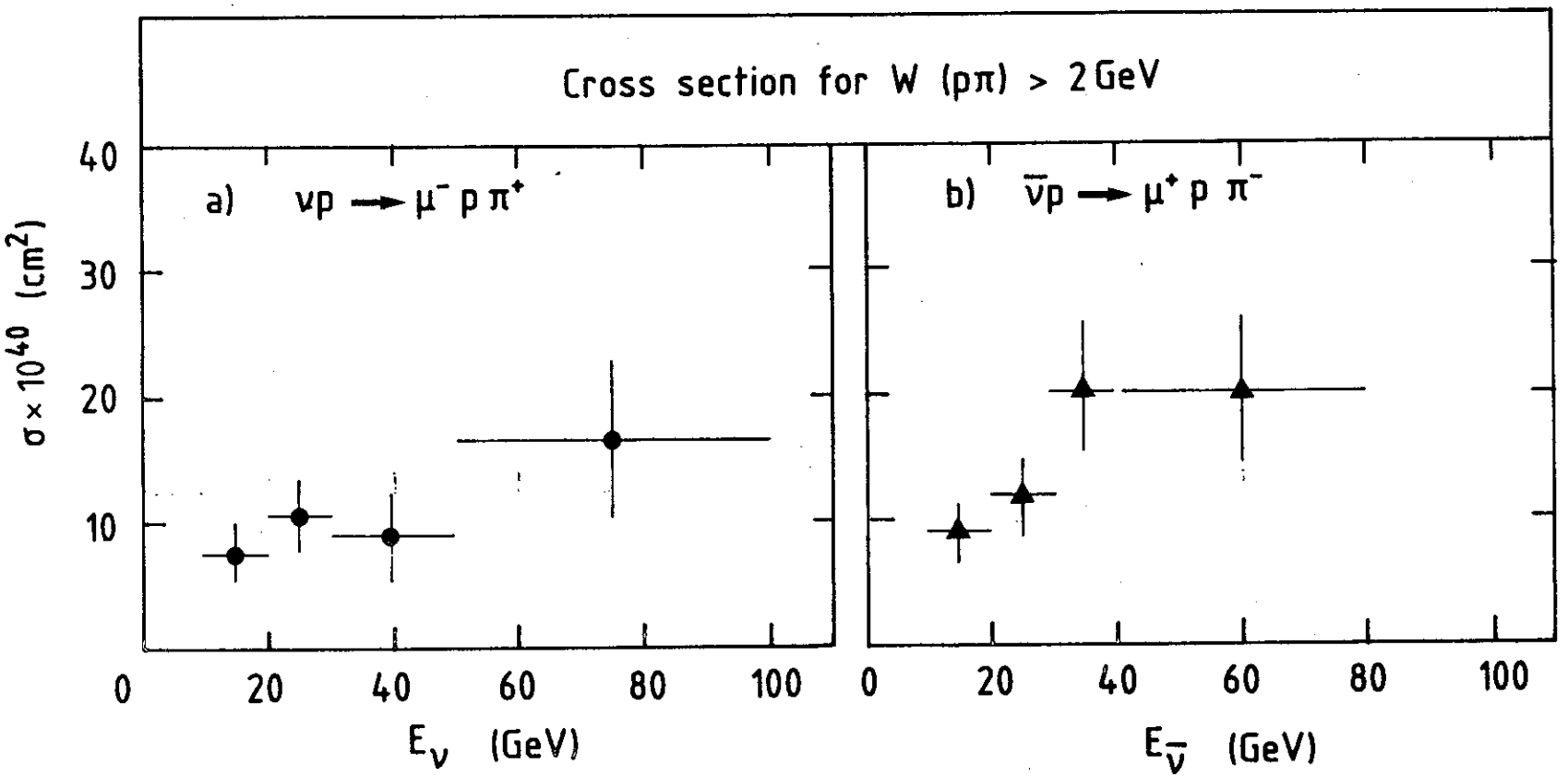
Cross section for W (pπ) > 2 GeV
a) νp → μ⁻ p π⁺
b) ν̄p → μ⁺ p π⁻
σ × 10⁴⁰ (cm²)
40
30
20
10
0
20
40
60
80
100
Eν (GeV)
Eν̄ (GeV)

Fig. 8

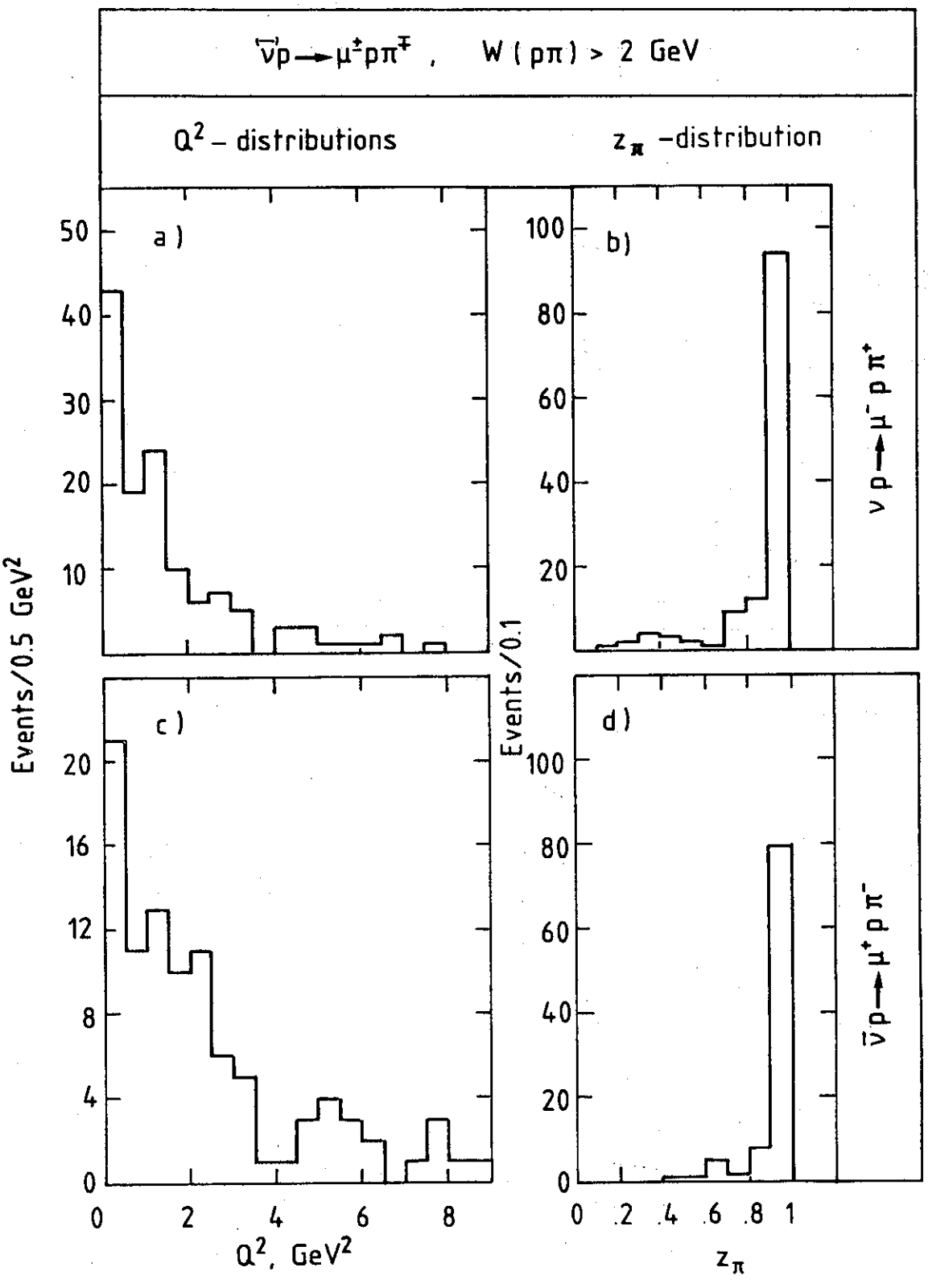
$\overleftarrow{\nu}p \rightarrow \mu^{\pm} p \pi^{\mp}$, W (pπ) > 2 GeV
Q^2 – distributions
z_π –distribution
a)
b)
c)
d)
Events/0.5 GeV^2
Events/0.1
Q^2, GeV^2
z_π
$\nu p \rightarrow \mu^- p \pi^+$
$\bar{\nu} p \rightarrow \mu^+ p \pi^-$

Fig. 9

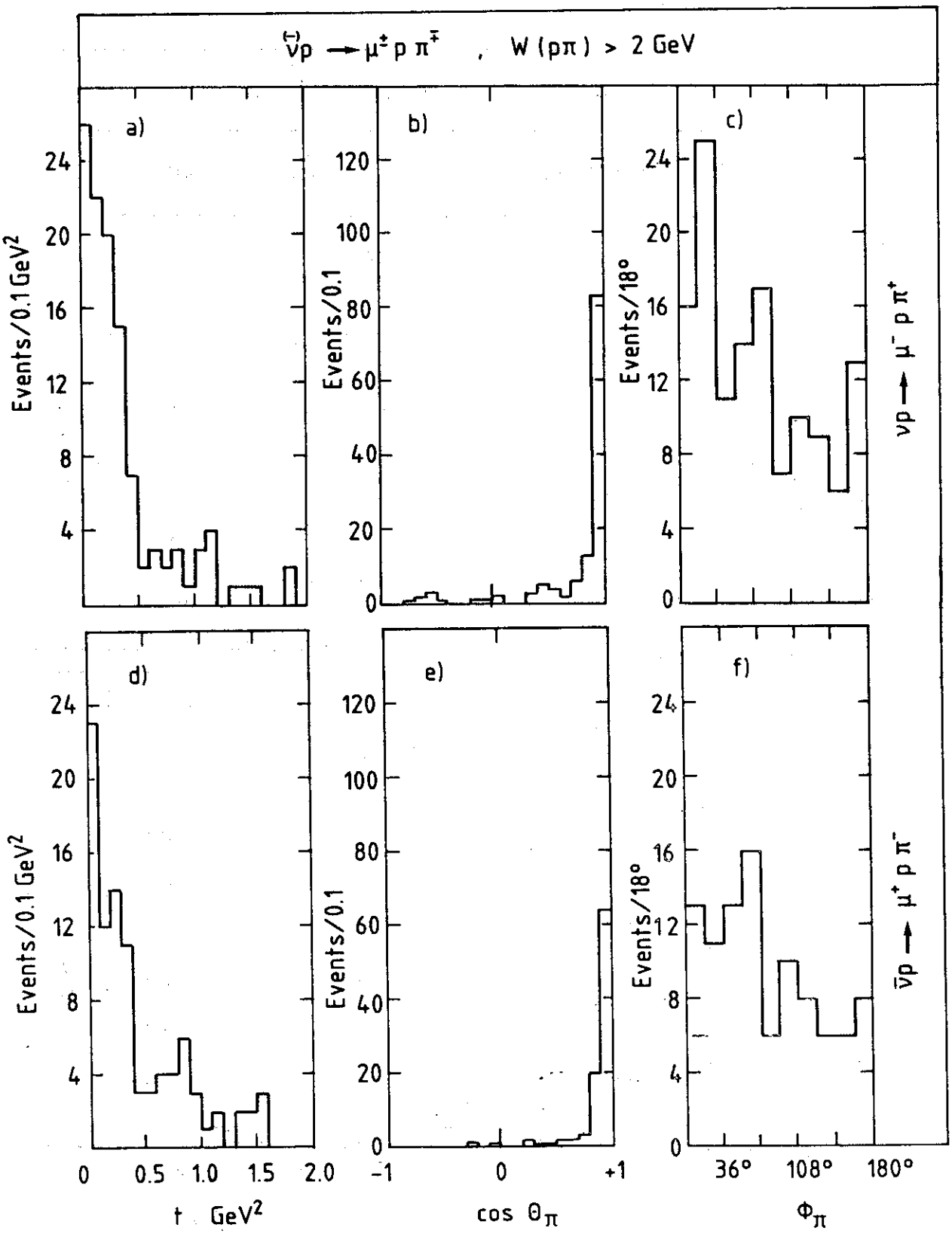
$\overset{(-)}{\nu}p \rightarrow \mu^{\pm} p \pi^{\mp}$, $W(p\pi) > 2$ GeV
a)
b)
c)
d)
e)
f)
Events/0.1 GeV²
Events/0.1
Events/18°
$\nu p \rightarrow \mu^- p \pi^+$
$\bar{\nu} p \rightarrow \mu^+ p \pi^-$
t GeV²
cos Θ_π
Φ_π
0
0.5
1.0
1.5
2.0
-1
+1
36°
108°
180°

Fig. 10

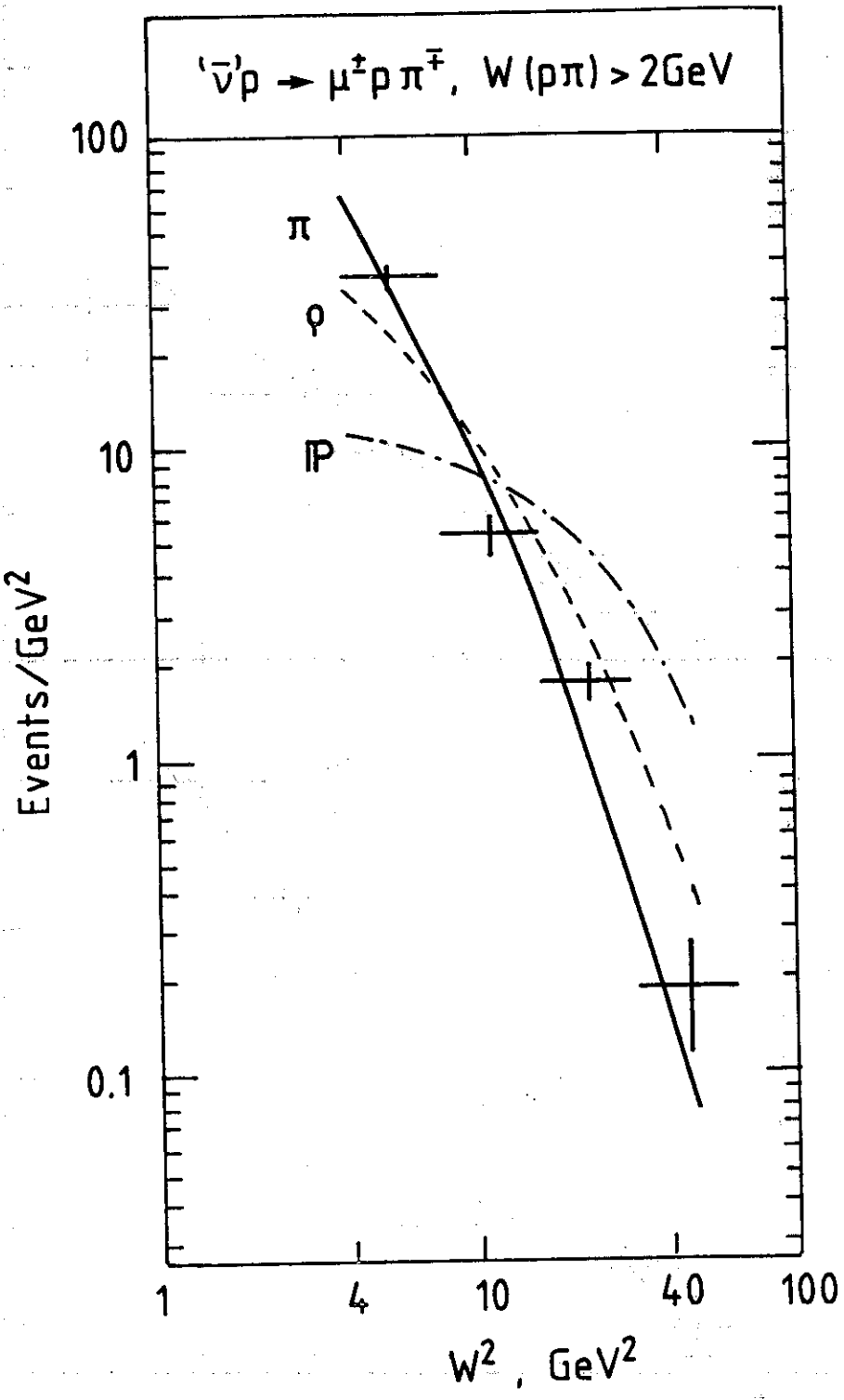

Fig. 11

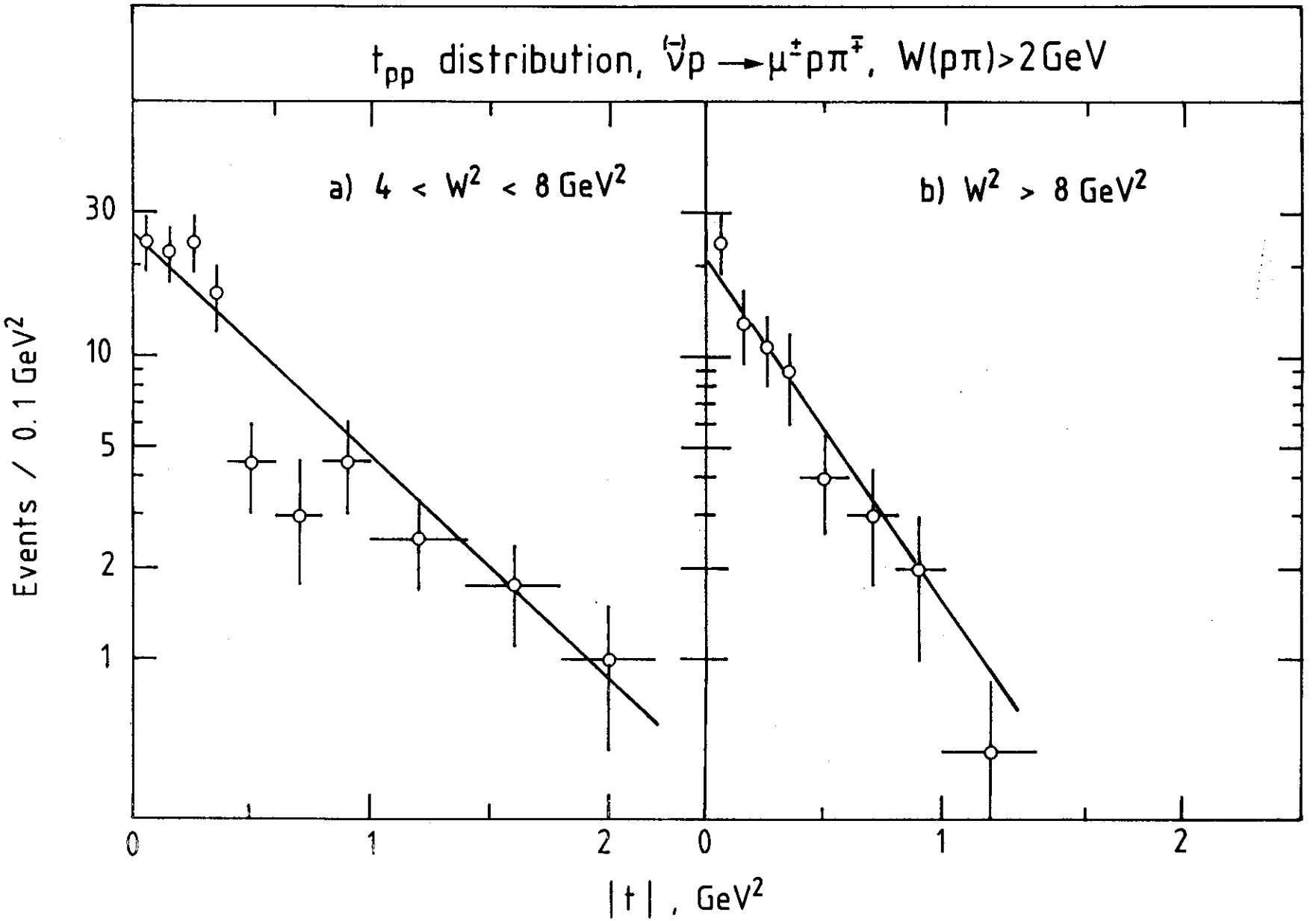
t_{pp} distribution, $\overset{(-)}{\nu}p \rightarrow \mu^{\pm}p\pi^{\mp}$, $W(p\pi)>2\,GeV$
a) $4 < W^2 < 8\,GeV^2$
b) $W^2 > 8\,GeV^2$
Events / 0.1 GeV^2
30
10
5
2
1
0
1
2
0
1
2
$|t|$, GeV^2

Fig. 12

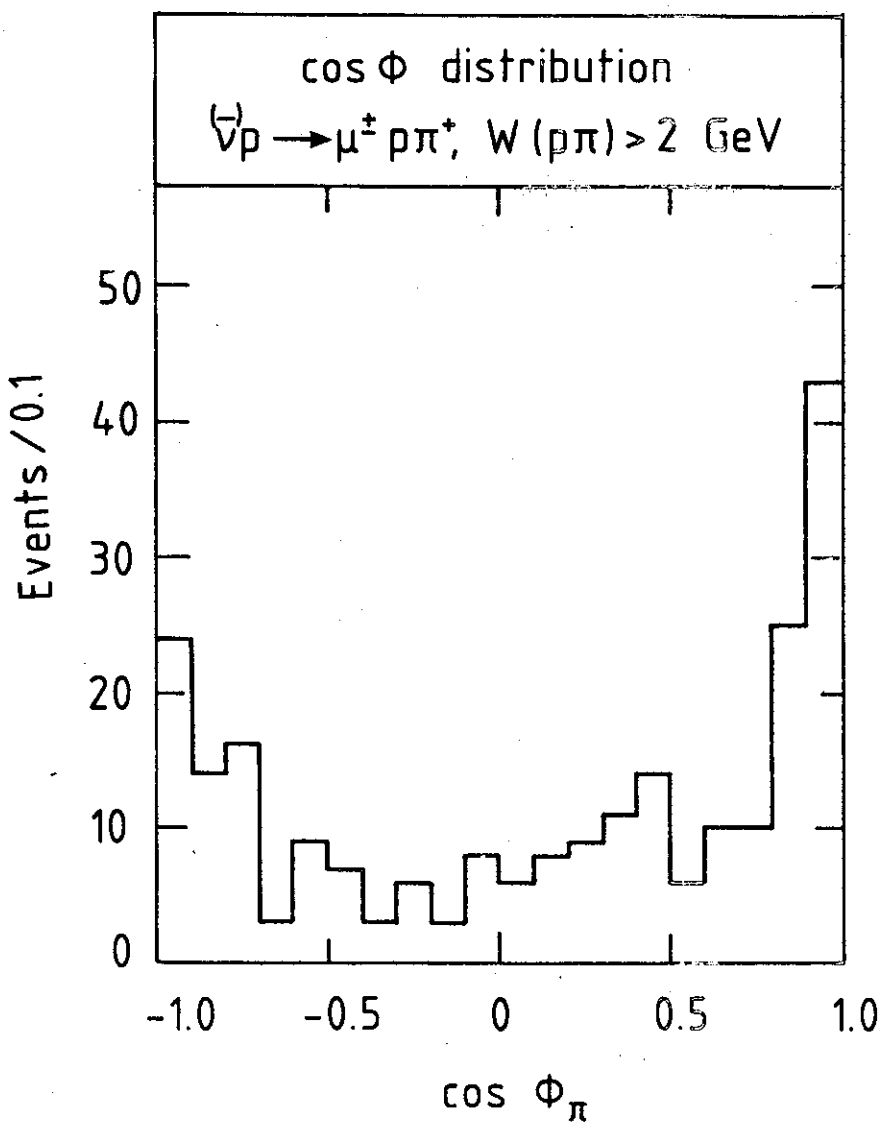
cos Φ distribution
$\overset{(-)}{\nu}p \rightarrow \mu^{\pm} p\pi^{+}$, W(pπ) > 2 GeV
Events / 0.1
50
40
30
20
10
0
-1.0
-0.5
0
0.5
1.0
cos Φ_{π}

Fig. 13

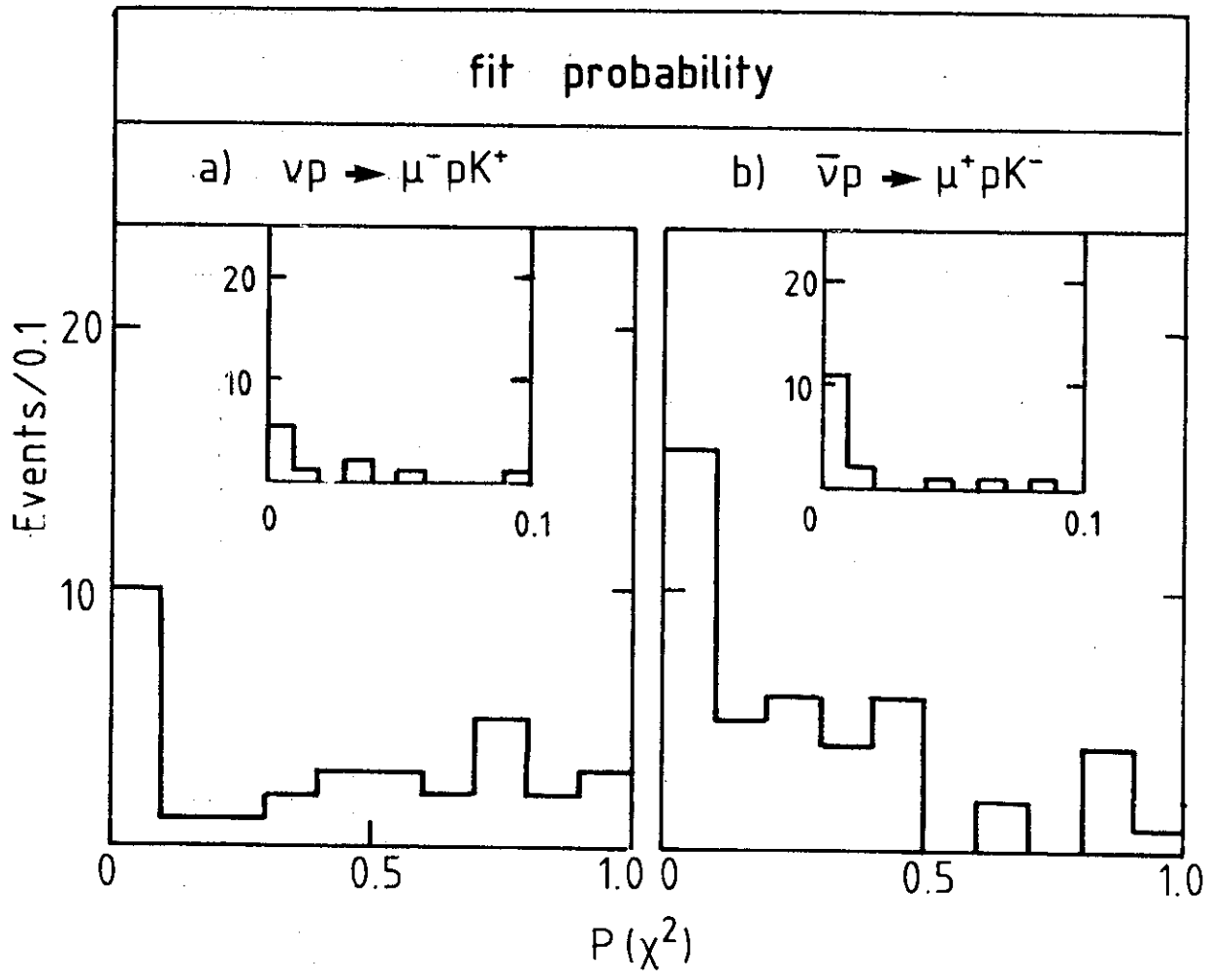

Fig. 14

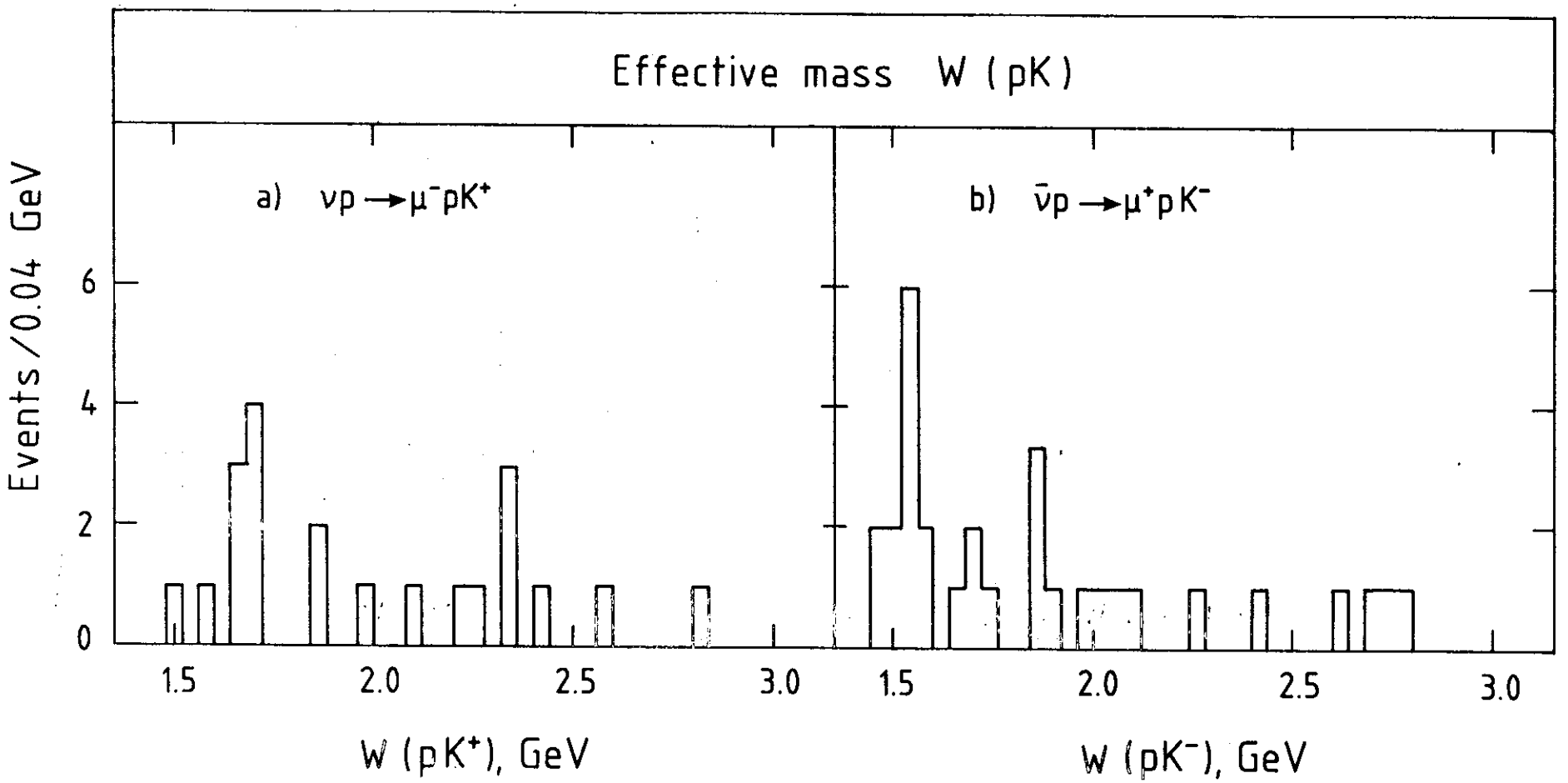
Effective mass W (pK)
a) νp → μ⁻pK⁺
b) ν̄p → μ⁺pK⁻
Events/0.04 GeV
0
2
4
6
1.5
2.0
2.5
3.0
W (pK⁺), GeV
W (pK⁻), GeV

Fig. 15